A sensitivity study of a FTIR retrieval algorithm to uncertainties in surface pressure measurements

S. NICOLAE[1,2], A. M. DANDOCSI[1,*], A. ILIE[1,3], C. RADU[1]
[1]*National Institute of Research and Development for Optoelectronics - INOE 2000, 409 Atomistilor St., 077125, Magurele, Romania*
[2]*UNST Politehnica of Bucharest, 1-3 Iuliu Maniu Blvd., Bucharest, 061071, Romania*
[3]*Faculty of Geography, University of Bucharest, 1 Nicolae Balcescu Blvd., 010041, Romania*

Greenhouse gases contribute to climate change through radiation forcing. To measure their quantities in the atmosphere, the Fourier Transform Infrared technique is being used. Within the Collaborative Carbon Column Observing Network, the raw signal is converted to column amounts of greenhouse gases through atmospheric inversion algorithms. Surface pressure data is required for the processing as a-priori information. This study presents a sensitivity study to surface pressure input data and the quantification of the error budget associated to the pressure input for the standard Collaborative Carbon Column Observing Network algorithm. Results show an inverse linear dependency between the pressure and retrieved quantity and an error estimation and post-processing correction factor is provided.

(Received April 15, 2025; accepted October 14, 2025)

Keywords: Fourier transform infrared, Greenhouse gases, Sensitivity study, Retrieval algorithm

1. Introduction

Optoelectronics is the study of electromagnetic radiation, specifically in the visible and near-visible range, and its accompanying transformation to electrical currents. Through continued developments in this field throughout the years, the technology implemented is being applied to the study of the atmosphere, used to measure the presence of various atmospheric constituents and the Earth's radiative budget [1,2] .

Greenhouse gases (GHGs) are the main driving factor of the warming of the Earth's atmosphere [3], contributing to a difference of 1.0-2.0°C to the pre-industrial era in the global surface temperature. Of this difference, 0.8°C and 0.5°C are attributed to atmospheric concentrations of CO_2 and CH_4, respectively [4].

The Paris Agreement [5] aims to limit GHG emissions, in order to limit the effect of global warming, up to a maximum of 2°C over pre-industrial era levels. Additional international agreements, such as the Global Methane Pledge [6] were adopted to ensure the mitigation of the effects of climate change.

In order to properly quantify the presence of GHGs and other atmospheric constituents in the atmosphere, different measurement techniques were developed, such as the Differential Optical Absorption Spectroscopy (DOAS) [7], or LiDAR [8-10]. One other such technique is Fourier Transform InfraRed (FTIR) spectroscopy, which is suitable for GHG column retrievals [11,12].

For proper evaluation of the total amount of different GHGs present in the atmosphere at regional/global scale, measurement networks have been formed, ensuring continuous and quality assured data provision respecting the FAIR principle. The COCCON network (Collaborative Carbon Column Observing Network) [13,14] consists of a multitude of FTIR instruments, ensuring interoperability and similar operating procedures to facilitate consistent and comparable measurements throughout its data.

In the retrieval process for FTIR data, a-priori information such as surface pressure, temperature and gas column profiles are required for obtaining GHG quantities from the measured spectra [15,16].

In this paper, a sensitivity study of the PROFFAST [15,16] retrieval algorithm is performed, in regards to the surface pressure measurements provided as a priori information.

Smith et al. [17] performed a study for Open-Path FTIR (OP-FTIR) utilizing gas cell measurements, with known parameters (gas concentration, pressure and temperature). They find an increase in the a priori assumed pressure of the gas cell leads to a decrease in the retrieved GHG quantities. This assumed pressure does not impact the spectral fit residuals significantly ($< \pm 0.04\%$), leading to an uncharacterized bias in the final retrieved quantities.

Furthermore, Guillaume et al. [18] studied the effect of assumed pressure in FTIR gas cell measurement for fire effluents. They find an acceptable tolerance of ±10 Torr ≈ 13.3 hPa for high concentrations of CO, where the maximum observed error for the retrieved concentration is 2.6%.

Therefore, a study for the sensitivity of OP-FTIR techniques is presented, quantifying the uncertainty in the retrieved GHG amounts as a function of input pressure variations. A COCCON-registered FTIR instrument [19] is utilized for obtaining the raw interferograms, and they are processed with the PROFFASTpylot [20] processing suite. Surface pressure data is obtained from a Lufft WS600-

UMB Smart Weather Sensor, with a stated accuracy of ±0.5 hPa at operating temperatures of 0-40°C [21].

The surface pressure measurements are modified and the retrieval procedure is run for each set of different input parameters.

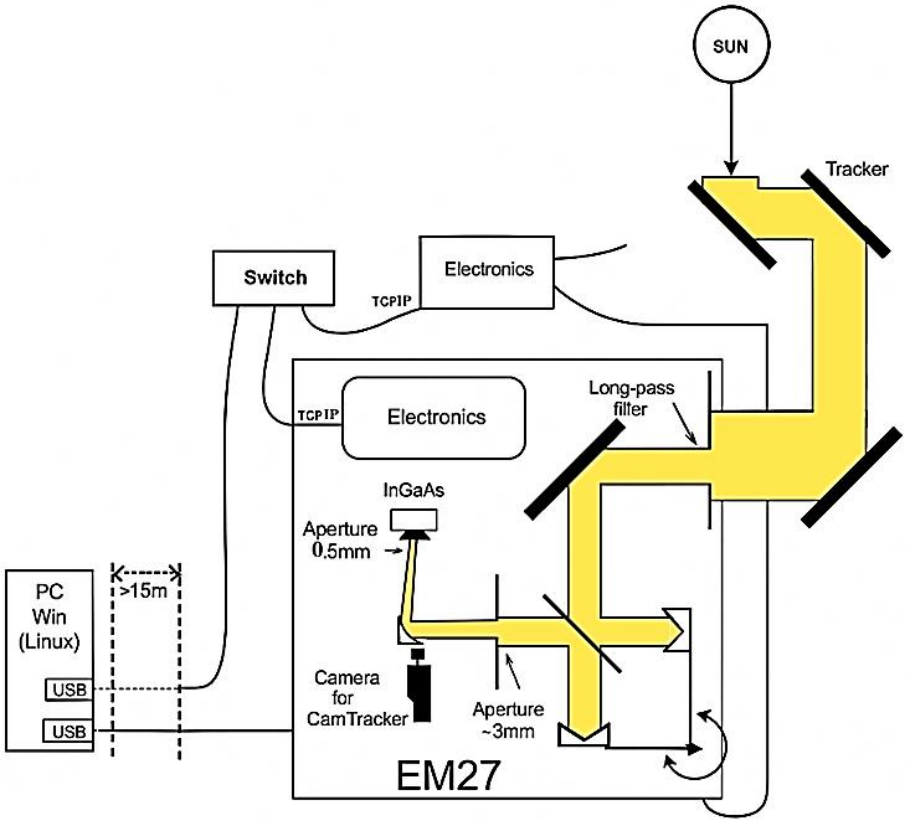

2. Instruments and software tools description

2.1. Bruker EM27/SUN

The Bruker EM27/SUN is a commercially available solar absorption FTIR spectrometer, co-developed with the Karlsruhe Institute for Technology [22] for the measurement and retrieval of atmospheric GHG concentrations. It is the standard instrument in the global COCCON network [19].

Fig. 1 presents a schematic drawing of the EM27/SUN spectrometer, featuring the optics, detector, and electronics part of the instrument. The spectrometer features a 0.5cm^{-1} resolution, achieved by introducing an optical path difference of 1.8cm along the two arms of the Michelson interferometer. It also features a portable design, weighing 25kg and measuring 35×40×27cm [23].

For this particular instrument, Mathias Frey estimates a 0.19% bias for a ±3 mbar pressure difference in the final retrieved trace gas column amounts [11]. Another bias estimate is 0.032% for the XCO_2 retrieval for +1 hPa in pressure [24].

The instrument also features a precision of 0.075% for XCO_2 and 0.057% for XCH_4 for 10min-running ifgs [24]. Gisi et al. [23] also finds the difference for a 34s averaged double-sided interferogram in XCO_2 measurements to be 0.20% ± 0.09%, when compared to standard TCCON measurements [25].

The operational measurements performed at the MARS site of INOE2000 [26-28] are done according to COCCON standards, acquiring 10 double-sided interferograms, with an integration period of 58s. The best estimation for the instrument's precision in this operation mode is 0.24% and 0.18% for the XCO_2 and XCH_4 retrievals, respectively, according to [24] and accounting for the difference in SNR compared to the 10-min interferogram acquisition mode.

2.2. PROFFAST and PROFFASTpylot

PROFFASTpylot [20] is an open-source software package aimed to automate the operation of the PROFFAST [29,30] software suite, used to process FTIR data.

The PROFFAST software suite is the standard processing procedure inside of the COCCON network. It features tools for preprocessing the FTIR data, computing the cross-sections of the constituents of the atmosphere at the time of measurement, and fitting the measured spectra over modelled ones based on a priori information. Fig. 2 highlights the main steps that are performed during the retrieval process:

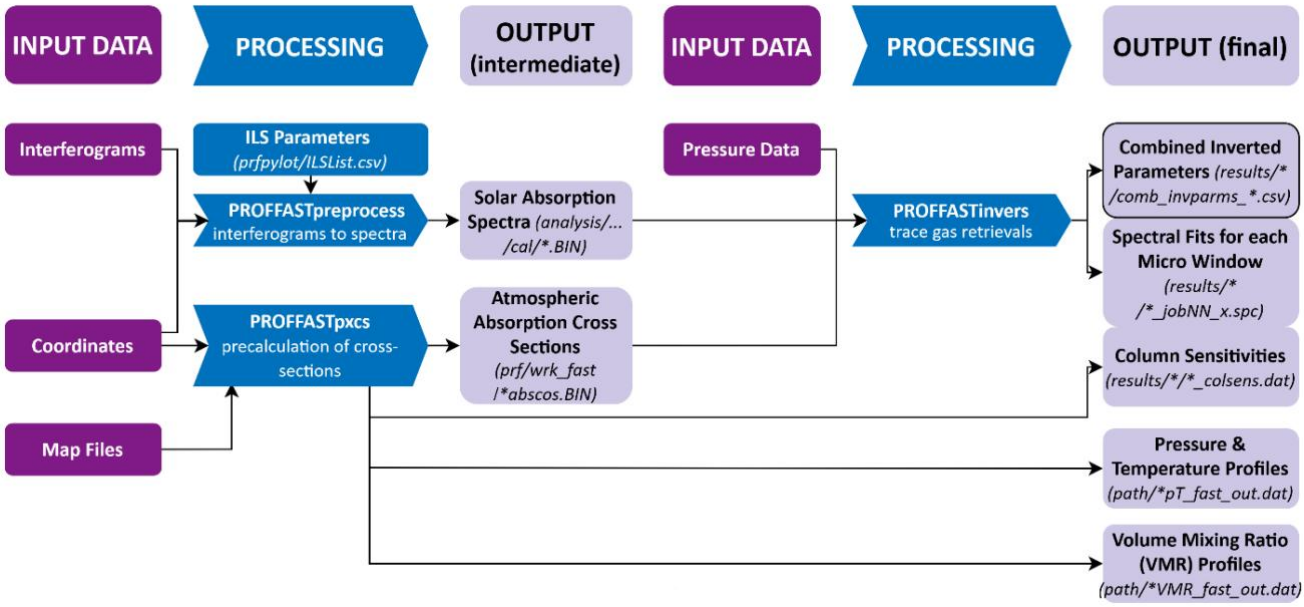

Fig. 2. Schematic representation of the PROFFASTpylot processing chain [15] (colour online)

1. "PROFFASTpreprocess": applies DC corrections to the instrumental signal and converts the measured interferograms into absorption spectra using the Fourier Transformation [31,32].
2. "PROFFASTpxcs": precomputes the cross-sections of different components of the atmosphere at the time of measurement.
3. "PROFFASTinvers": models spectra based on precomputed cross sections and fits the measured spectra over these. Produces the final trace gas retrievals.

PROFFAST requires 3 different types of input data for a successful retrieval. These are:

1. Interferograms measured by the instrument. These are obtained with the OPUS software suite, version 7.5 [33]. Alternatively, ready-preprocessed spectra can be used.
2. A priori pressure measurements collocated with the instrument. These ideally have sufficient time resolution and with a precision of ±0.2 mbar [15] in order to avoid additional errors in the retrieval process.
3. A priori column distribution profiles of atmospheric constituents. These are obtained from the GEOS-FP or GEOS-FPIT models [34]. These files are commonly referred to as GGG2014 (daily frequency) or GGG2020 (3-hour frequency) files, also being used in the standard TCCON retrieval process [35].

In this study, we will utilize GGG2020 files from the GEOS-FP as input for the processing chain.

3. Methodology

3.1. Pressure measurements

Site collocated surface pressure measurements are obtained with the utilization of a Lufft WS600-UMB Smart Weather Sensor [21]. The stated accuracy of the sensor is ±0.5 hPa at operating temperatures of 0-40°C and the temporal frequency is 1 minute.

In order to study the effects of surface pressure measurements' values in the final retrieved quantities of trace gas constituents, the entire retrieval process has been rerun with modified pressure data.

The reference values consist of the operationally processed data, utilizing unmodified pressure files from the sensor. The following cases have been studied, for each of the retrieved GHG column amounts:

1. 0.1% positive bias (≈ +1hPa in normal weather conditions)
2. 0.1% negative bias (≈ -1hPa in normal weather conditions)
3. 5 different 0.05% random bias (-0.5hPa to +0.5hPa range in normal weather conditions)
4. +1hPa positive offset
5. -1hPa negative offset
6. +50 hPa positive offset
7. -50 hPa negative offset

The values of 0.1%, 0.05% biases and 1hPa offsets in either direction were chosen as they are close to the precisions or biases offered by commercially available pressure sensors [36-38]. Since the FTIR instrument does not have a built-in pressure sensor, it is the user's responsibility to provide the data. Therefore, understanding and quantifying the possible uncertainties coming from incoherent pressure data is important for assuring properly retrieved GHG quantities.

The 50 hPa offsets were chosen due to the possible inaccuracy of the a priori profile. For example, in real life measurements, if a plume is modelled at height z and the modelled spectrum precomputed accounts for said plume, the PROFFASTinvers program will try to fit the spectral response of the instrument for said plume at pressure $p(z)$, accounting for effects such as pressure line broadening [39]. However, if in reality the plume is higher (or lower) in the

atmosphere, with the height difference *Δz*, the *p(z)* pressure changes to become *p(z+Δz)*. In such cases, and when Δz is expressed in km, a good approximation for the pressure shift is [17]:

$$p(z + \Delta z) = p(z) + 100 \cdot \Delta z \; [hPa] \quad (1)$$

As such, a 50hPa offset accounts for a 0.5km bias in the height of the measured plume. This is a rough approximation, as this only accounts for a segmented plume out of the total column measurements. In reality, this is an edge case of the inaccuracies which would come from height uncertainties of plumes' heights.

3.2. Measurements and data processing

The standard COCCON measurement procedure was employed for obtaining the raw interferograms. Details about the configuration can be found at [40] and include settings of the instrument, as well as the software tools required for the measurements.

For this study, 107 days of measurements from the year 2024 were utilized. For each different pressure input, the entire processing chain was run, producing the final retrieval quantities.

Processing data was done with the PROFFASTpylot software suite (PROFFASTpylot v1.3 and PROFFAST v2.4) [20], and the handling of the pressure input data was done through a mix of Python [41] (e.g., for the random bias case) functions and in-built functionality of the PROFFASTpylot software suite.

The studied gaseous compounds are total column amounts of CO_2, CH_4, CO and water vapor (H_2O). The processing chain also outputs volume mixing ratios (VMRs) of these compounds, but these are additionally sensitive to pressure differences in the input data, as the VMR of a compound, when the distribution inside of the atmospheric column is uniform, is calculated as [17]:

$$VMR = \frac{X \cdot R \cdot T}{h \cdot p \cdot A} \quad (2)$$

where VMR is the volume mixing ratio, in ppm, X is the column amount in molecules/cm^2, $R = 8.314 \frac{J}{mol \cdot K}$ is the gas constant, T is the temperature in K, h is the height of the atmospheric column in m, p is the pressure in hPa and $A = 6.022 \cdot 10^{23} mol^{-1}$ is Avogadro's constant.

This makes VMRs unsuitable for a comparison, as we introduce additional, unwanted bias and uncertainties (compared to total column values), especially since the distribution inside the atmospheric column is not uniform and is different for each gaseous compound.

3.3. Post-processing and statistical analysis

A post-processing routine has been applied to the retrieved GHG column amounts, involving deseasonalizing the data, utilizing a Lomb-Scargle periodogram [42]. This step ensures consistency when inferring a dependency of final retrieved quantities on surface pressure measurements, eliminating unwanted time-related biases from the retrieval of greenhouse gas quantities [43,44]. In this approach, only the highest amplitude frequency component (with $\nu > 1$ day) has been removed in order to preserve intra-day variability of greenhouse gases total column amount.

For analyzing the differences in the final retrieved quantities for each case, a metric of relative differences is implemented. This is defined as:

$$RD = \frac{X - X_0}{X_0} \cdot 100 \; [\%] \quad (3)$$

where X is the retrieved GHG quantity with the modified pressure files and X_0 is the original retrieved GHG quantity.

Additionally, a qualitative analysis of the influence of the solar zenith angle (further referred to as SZA) on the retrieved quantities is performed. The SZA influences the retrieved column amounts by influencing the air mass factor (AMF), a parameter which describes the ratio of GHG between the retrieved slant column and the vertical column. The relationship between the AMF and the SZA is described by an inverse cosine function [45]:

$$AMF = \frac{1}{\cos(SZA)} \quad (4)$$

Since the SZA-induced bias is a direct consequence of the retrieval process, and is directly influenced by a difference in pressure, only a qualitative analysis will be performed for it. This step involves computing the inverse-cosine dependency of retrieved values from each different measurement day and then subtracting it from the data. The main goal of this procedure is to help properly visualize the direct dependencies between surface pressure and retrieved quantities, without additional variability introduced by other variables.

4. Results

4.1. Carbon dioxide retrieval results

Fig. 3 shows the results of the retrieval of total column CO_2 for a single day of measurements. The relative differences are expressed as a function of the difference in surface pressure between the initial, unmodified retrieval and the modified retrieval. An inverse-cosine-like dependence is seen, which supports the assumed dependence of the retrieved relative difference and the SZA (see eq. (4)).

Since this dependency is present in all days of measurement, and the variation interval for the SZA is similar for each day, a similar shape for the relative difference is expected for each continuous measurement. This can be seen in Fig. 4, where a multitude of such inverse-cosine-like shapes can be seen.

Furthermore, the dependency to the SZA is statistically canceled out on average due to its reproductible behaviour in time. Therefore, a linear fit is provided alongside the data points, in Fig. 4 and Fig. 5. This quantifies the dependency between the difference in surface pressure used for the retrieval and the final retrieved differences.

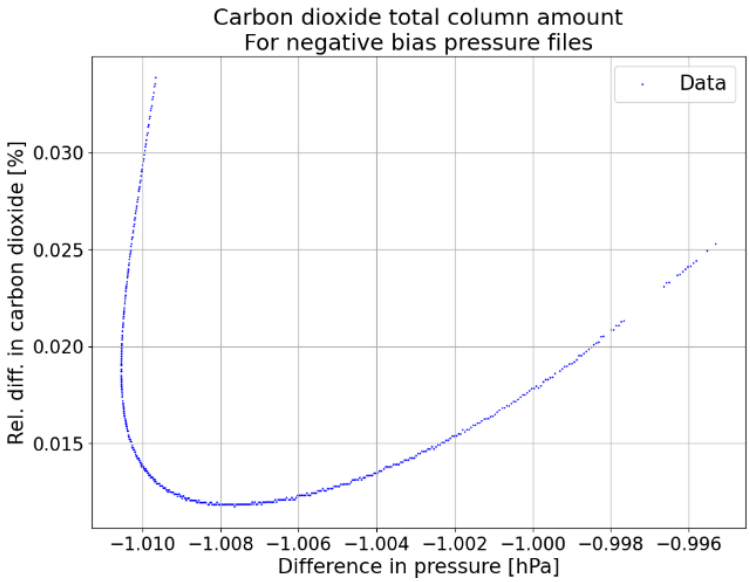

Fig. 3. Retrieval results for carbon dioxide, for a single day of measurements, utilizing an artificial 0.1% negative bias introduced in the surface pressure measurements (colour online)

Fig. 4 and Fig. 5 show that an inverse relationship between the difference in surface pressure and final retrieved quantities is present, when processing is done with bias-modified pressure files. For both the negative-bias and positive-bias cases, the regression slope can be expressed as:

$$RD = -1.75 \cdot 10^{-2} \cdot \Delta p \ [\%] \tag{5}$$

where Δp is the difference in pressure. These results indicate a relative difference of -0.0175% for an offset of +1 hPa in the assumed surface pressure. This is in good agreement with the findings from the ± 1 hPa offset-processed cases, shown in Fig. 6 and Fig. 7, which highlight mean relative differences of -0.017% (for a +1 hPa offset) and 0.018% (for a -1 hPa offset).

Therefore, a scaling factor for the ± 1 hPa interval is proposed as follows:

$$S = \frac{\mu_{RD}}{\Delta p} = \frac{-0.0175\%}{hPa} \tag{6}$$

where S is calculated as the average of the values obtained with eq. (6) from both of the ± 1 hPa offset-processed cases.

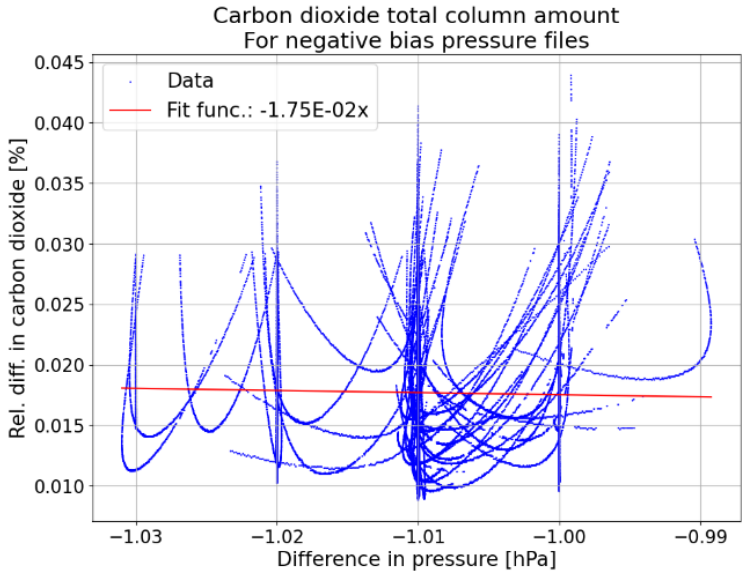

Fig. 4. Retrieved relative difference of total column carbon dioxide amount utilizing processing with an artificial 0.1% negative bias introduced in the surface pressure measurements (colour online)

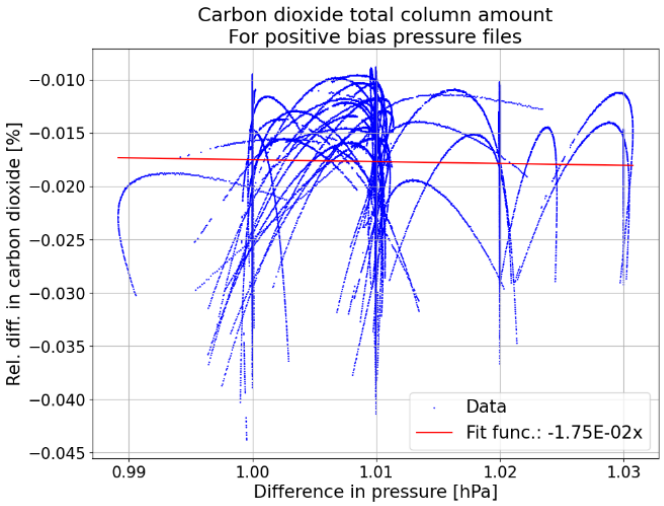

Fig. 5. Retrieved relative difference of total column carbon dioxide amount utilizing processing with an artificial 0.1% positive bias introduced in the surface pressure measurements (colour online)

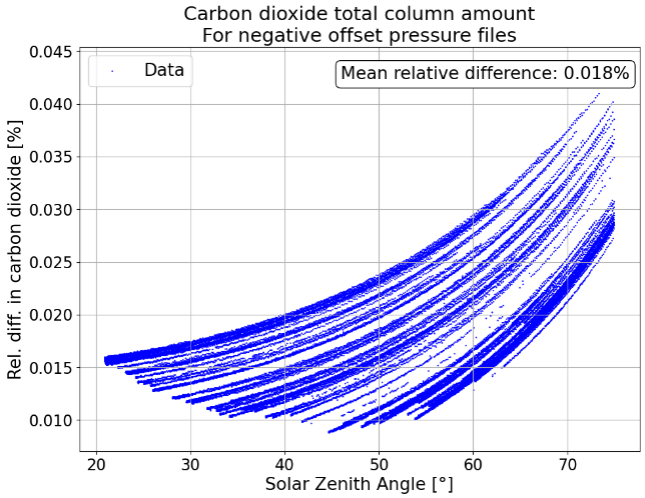

Fig. 6. Retrieved relative difference of total column carbon dioxide amount utilizing processing with an artificial 1 hPa negative offset introduced in the surface pressure measurements, shown in relation to the solar zenith angle (colour online)

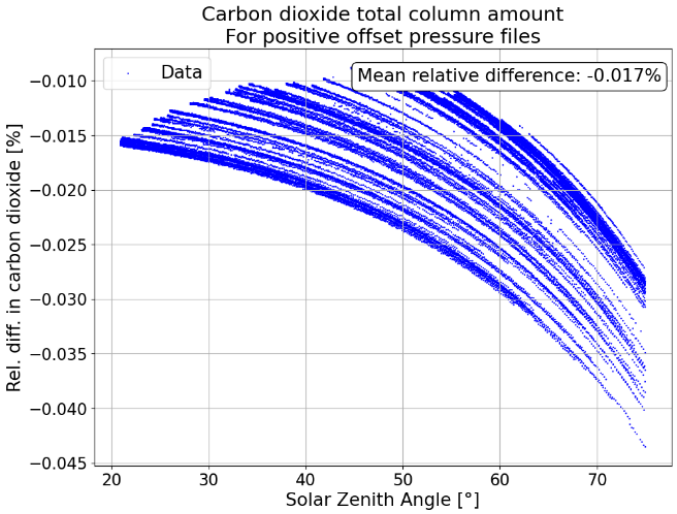

Fig. 7. Retrieved relative difference of total column carbon dioxide amount utilizing processing with an artificial 1 hPa positive offset introduced in the surface pressure measurements, shown in relation to the solar zenith angle (colour online)

Following methodology explained in Section 3.1., a study on noisy surface pressure input data has also been done, introducing a 0.05% random bias in the pressure data. The results indicate a mean standard deviation of $4.45 \cdot 10^{21}$ molec/cm^2 and a mean value of $9.06 \cdot 10^{25}$ molec/cm^2 across the 5 reruns of the processing chain. Therefore, the mean relative standard deviation can be calculated as:

$$\sigma_{RD} = \frac{\sigma_X}{\mu_X} \approx 4.91 \cdot 10^{-3}\ [\%] \quad (7)$$

The processing results for the entire timespan of the study are shown below, in Fig. 8.

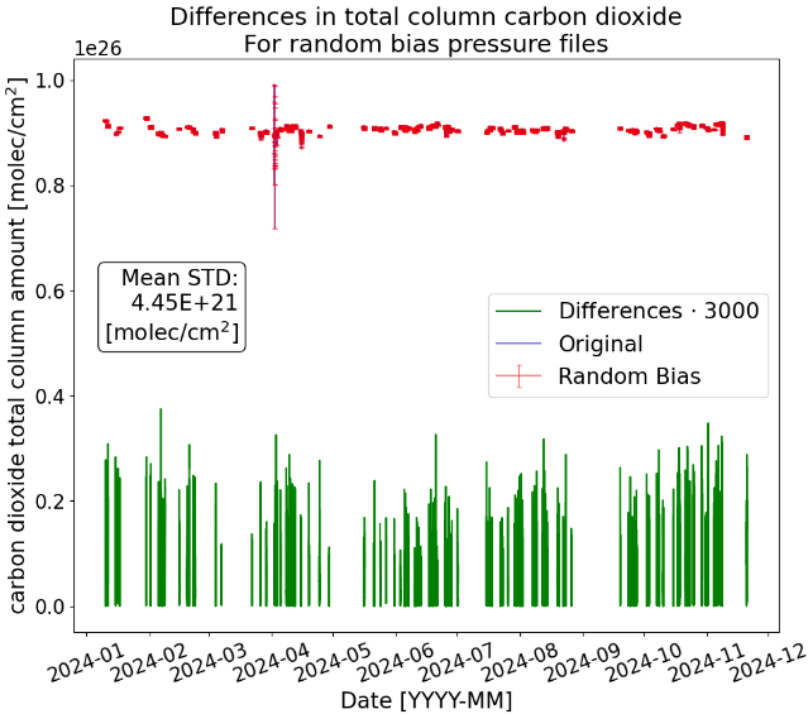

Fig. 8. Retrieved relative difference of total column carbon dioxide amount utilizing processing with an artificial 0.05% random bias introduced in the surface pressure measurements (colour online)

Additionally, the processing was also run with a ±50hPa offset, as seen in Figs. 9 and 10. The results show a mean relative difference of +0.902% (for a -50hPa offset) and -0.854% (for a +50hPa offset), indicating a small asymmetry between the two cases. However, utilizing eq. (6), the approximation for the scaling factors becomes:

$$S_{positive-offset} = \frac{-0.854\%}{50} \approx -0.017\ \left[\frac{\%}{hPa}\right] \quad (8)$$

$$S_{negative-offset} = \frac{0.902\%}{-50} \approx -0.018\ \left[\frac{\%}{hPa}\right] \quad (9)$$

This leads to a final approximation of the scaling factor as:

$$S_{big-offset} = \frac{-0.017 - 0.018}{2} = -0.0175\ \left[\frac{\%}{hPa}\right] \quad (10)$$

The value is consistent with the scaling factor obtained in eq. (6), highlighting a near-linear dependency of total column amount of CO_2 to the difference in surface pressure used for the retrieval process.

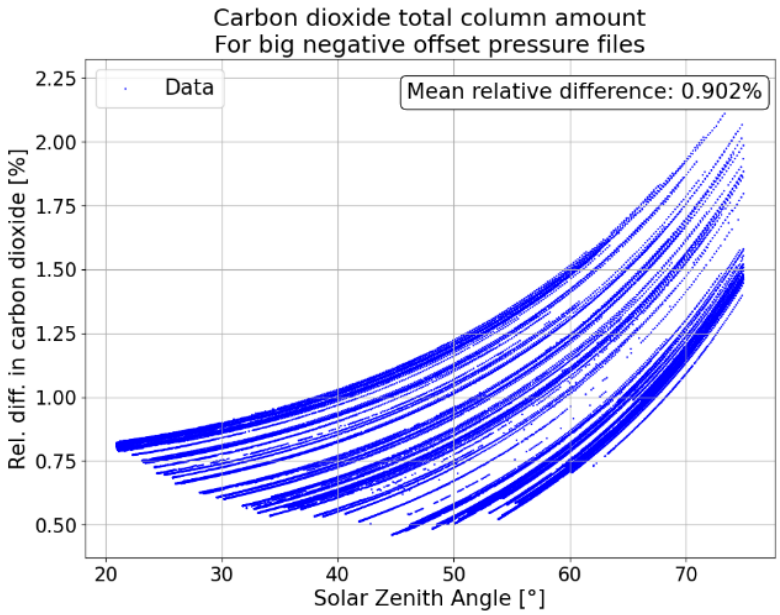

Fig. 9. Retrieved relative difference of total column carbon dioxide amount utilizing processing with an artificial 50 hPa negative offset introduced in the surface pressure measurements, shown in relation to the solar zenith angle (colour online)

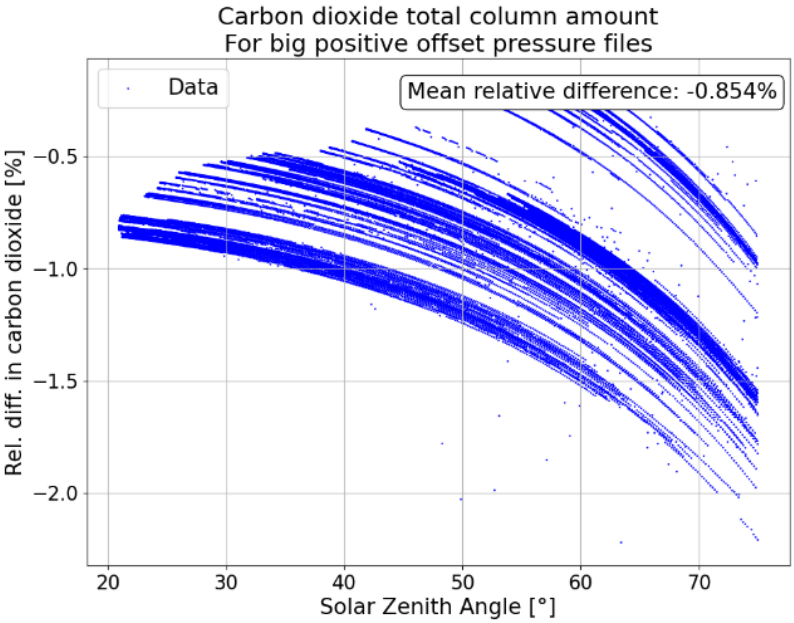

Fig. 10. Retrieved relative difference of total column carbon dioxide amount utilizing processing with an artificial 50 hPa positive offset introduced in the surface pressure measurements, shown in relation to the solar zenith angle (colour online)

Furthermore, Fig. 11 and Fig. 12 show the results after the SZA-induced bias was removed from the results.

A preliminary analysis on the retrieved slope (see eq. (5)) shows a good agreement with the bias-processed results, indicating good consistency between the two cases.

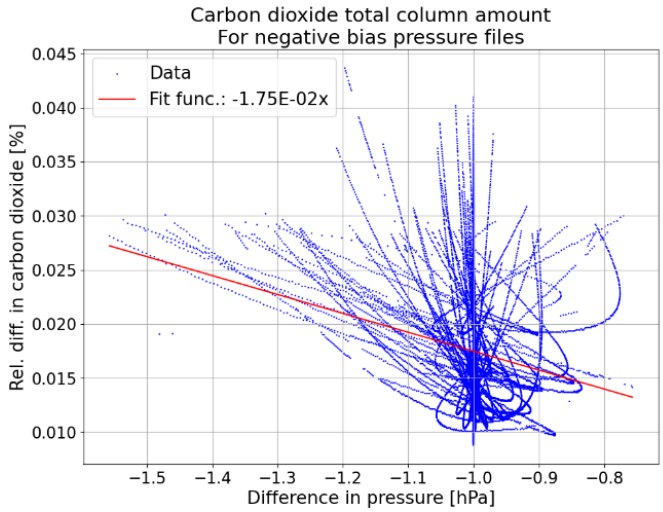

Fig. 11. Retrieved relative difference of total column carbon dioxide amount utilizing processing with an artificial 0.1% negative bias introduced in the surface pressure measurements, and the SZA-induced bias removed (colour online)

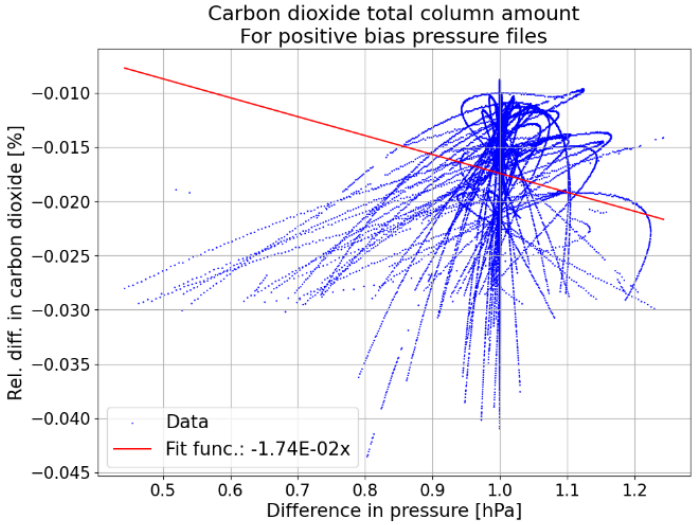

Fig. 12. Retrieved relative difference of total column carbon dioxide amount utilizing processing with an artificial 0.1% negative bias introduced in the surface pressure measurements, and the SZA-induced bias removed (colour online)

4.2. Methane retrieval results

Methane retrievals present similar qualitative characteristics as carbon dioxide retrievals, showing an inverse dependency of final retrieved GHG total column amount in regards to the input pressure utilized.

A similar behavior to the carbon dioxide retrieval as the retrieval for carbon dioxide is observed and leads to a mean relative difference of $\mp 0.014\%$ for a ± 1hPa offset in pressure. Thus, the scaling factor utilized defined in eq. (6) becomes:

$$S = \frac{\mu_{RD}}{\Delta p} = \frac{-0.014\%}{hPa} \tag{11}$$

These findings are also supported by the $\pm 0.1\%$ bias-processed retrieval quantities, with the linear fit, similar to eq. (5) becoming:

$$RD = -1.37 \cdot 10^{-2} \cdot \Delta p \ [\%] \tag{12}$$

where RD is the relative difference, and Δp is the difference in pressure.

When analyzing the ± 50hPa offset-processed results, shown in Figs. 16 and 17, a mean relative difference of +0.699% (for -50hPa offset) and -0.669% (for +50hPa offset) is found. This is consistent with the ± 1hPa offset data, leading to two slightly asymmetrical scaling factors:

$$S_{positive-offset} = \frac{-0.669\%}{50} \approx -0.013 \left[\frac{\%}{hPa}\right] \tag{13}$$

$$S_{negative-offset} = \frac{0.699\%}{-50} = -0.014 \left[\frac{\%}{hPa}\right] \quad (14)$$

Overall, according to eq. (10), this can be quantified with the average scaling factor of:

$$S_{big-offset} = \frac{-0.013 - 0.014}{2} = -0.0135 \left[\frac{\%}{hPa}\right] \quad (15)$$

Following the same 0.05% random bias processing procedure as for CO_2, the results obtained are those from Fig. 13, with a mean standard deviation of $1.58 \cdot 10^{19}$ molec/cm^2 and a mean value of $4.15 \cdot 10^{24}$ molec/cm^2. A relative standard deviation is also found by substituting the new values in eq. (7):

$$\sigma_{RD} = \frac{\sigma_X}{\mu_X} \approx 3.81 \cdot 10^{-3} \, [\%] \quad (16)$$

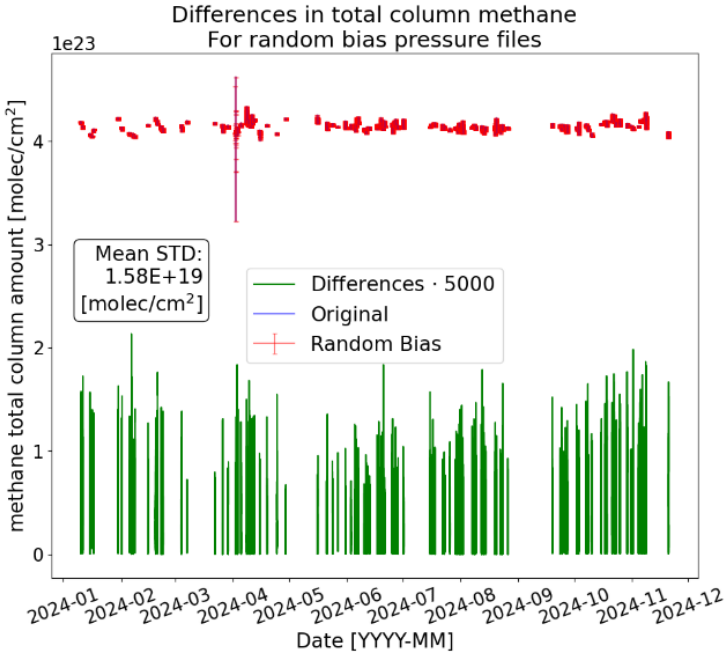

Fig. 13. Retrieved relative difference of total column methane amount utilizing processing with an artificial 0.05% random bias introduced in the surface pressure measurements (colour online)

Additionally, ±0.1% bias-processed files are shown in Fig. 14 and Fig. 15, with the solar zenith angle induced variation removed. These highlight a similar trend of ∓0.0137% differences compared to original files, being consistent with the findings from the unmodified bias-processed files.

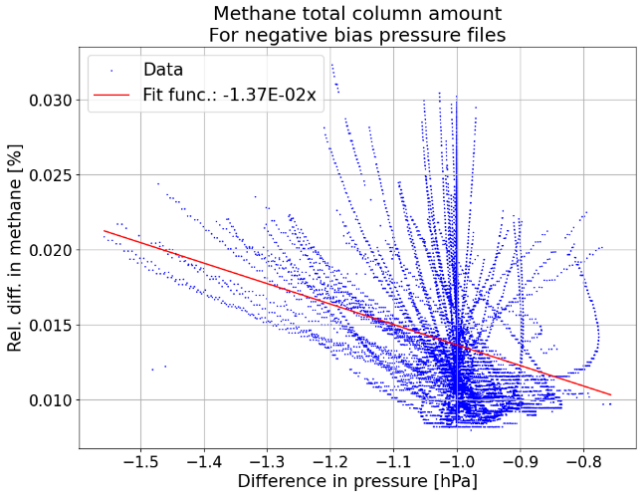

Fig. 14. Retrieved relative difference of total column methane amount utilizing processing with an artificial 0.1% negative bias introduced in the surface pressure measurements, and with the SZA-induced bias removed from the final data (colour online)

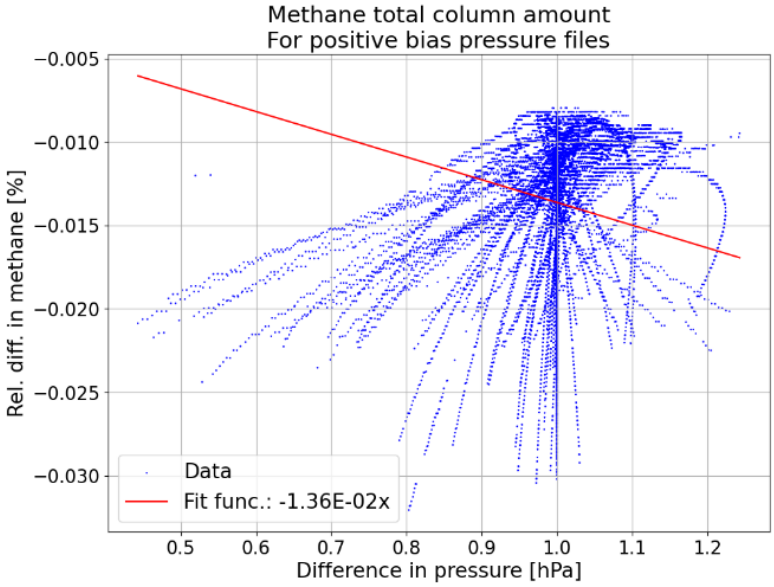

Fig. 15. Retrieved relative difference of total column methane amount utilizing processing with an artificial 0.1% positive bias introduced in the surface pressure measurements, and with the SZA-induced bias removed from the final data (colour online)

4.3. Carbon monoxide retrieval results

Similarly to methane and carbon dioxide, carbon monoxide retrievals show an inverse dependency on the surface pressure measurements used as an input.

However, both the mean relative differences in the offset-processed retrievals (eq. (6)) and the regression slope in the bias-processed retrievals (eq. (5)) show a weaker dependency on surface pressure, with lower absolute values:

$$S = \frac{\mu_{RD}}{\Delta p} = \frac{-0.008\%}{hPa} \tag{17}$$

$$RD = -7.94 \cdot 10^{-3} \cdot \Delta p \ [\%] \tag{18}$$

Furthermore, the intraday variability of carbon monoxide is higher than for other trace gases, given its shorter lifespan of 2-4 months in the atmosphere [46], compared to other GHGs. This can be seen in the example provided in Fig. 16, where the data points are more scattered than for the carbon dioxide and methane retrieval results.

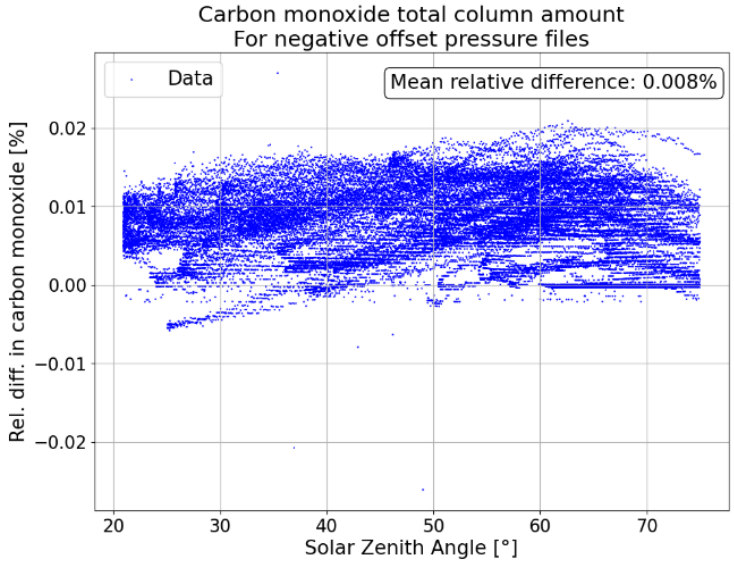

Fig. 16. Retrieved relative difference of total column carbon monoxide amount utilising processing with an artificial 1 hPa znegative offset introduced in the surface pressure measurements, shown in relation to the solar zenith angle (colour online)

As for methane and carbon dioxide, a study on $\pm 0.05\%$ random bias-processed files were concluded, showing a mean standard deviation of $4.93 \cdot 10^{17}$ molec/cm^2 and a mean value of $2.11 \cdot 10^{22}$ molec/cm^2. The results are presented in Fig. 17.

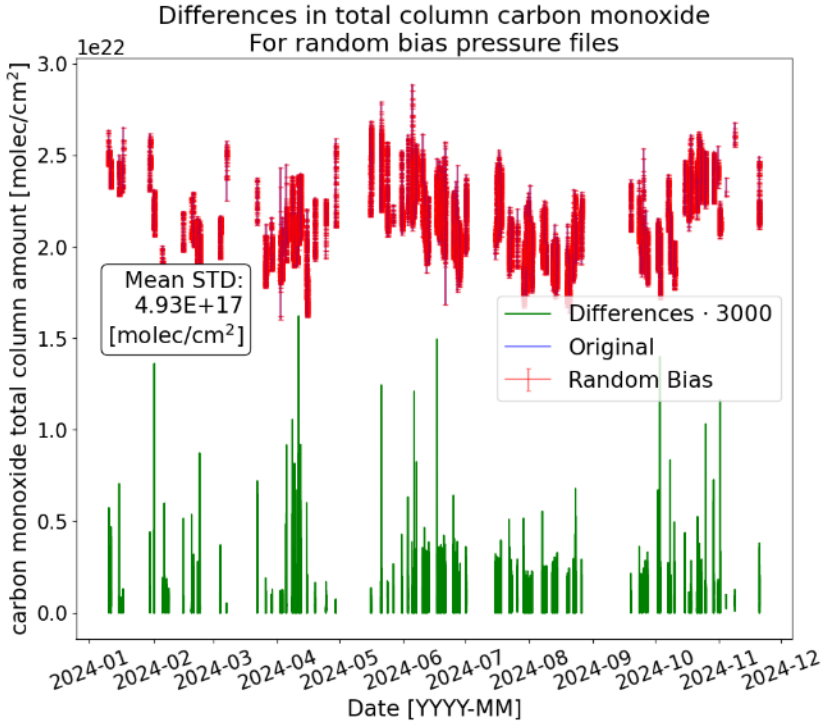

Fig. 17. Retrieved relative difference of total column carbon monoxide amount utilizing processing with an artificial 0.05% random bias introduced in the surface pressure measurements (colour online)

Utilizing eq. (7), the relative standard deviation is:

$$\sigma_{RD} = \frac{\sigma_X}{\mu_X} \approx 2.34 \cdot 10^{-3}\ [\%] \tag{19}$$

For the case of a ± 50 hPa offset applied to the surface pressure measurements, a similar behavior to the smaller offset case is seen. Variability is still high, and the data present a +0.406% bias (for a -50hPa offset) and -0.389% bias (for a +50hPa offset), respectively. This leads to two slightly asymmetrical scaling factors:

$$S_{positive-offset} = \frac{-0.389\%}{50} \approx -0.008\ \left[\frac{\%}{hPa}\right] \tag{20}$$

$$S_{negative-offset} = \frac{0.406\%}{-50} \approx -0.008\ \left[\frac{\%}{hPa}\right] \tag{21}$$

With the help of eq. (10), a scaling factor is proposed with the following value:

$$S_{big-offset} = \frac{-0.008 - 0.008}{2} = -0.008\ \left[\frac{\%}{hPa}\right] \tag{22}$$

This is consistent with the inverse linear dependence observed in the aforementioned cases, thus supporting the idea that the inverse linear dependency is extendable to a ± 50 hPa offset in assumed pressure.

Additionally, $\pm 0.1\%$ bias-processed files are shown in fig. 19 and fig. 20, with the solar zenith angle induced variation removed. These highlight a similar trend of $\mp 0.008\%$ differences compared to original files, in accordance with the results from the bias-processed files. This supports the idea that the linear dependency comes from the pressure variation, and not another uncharacterized dependency, such as intraday variability, which is partly accounted for by removing the SZA-induced component.

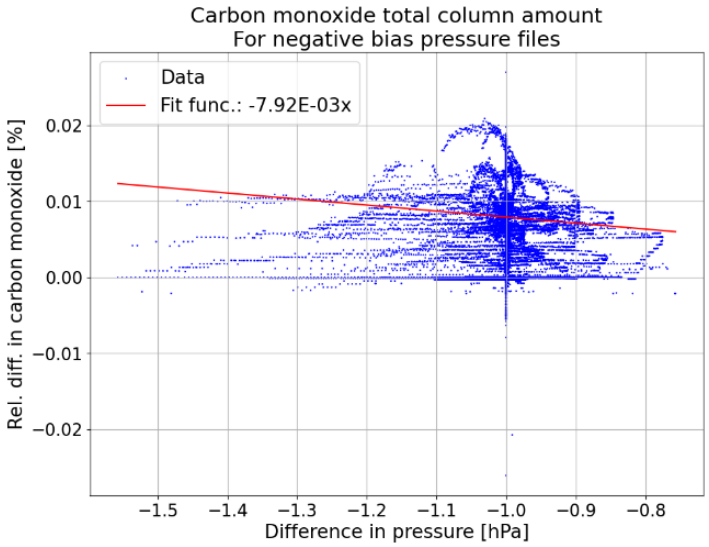

Fig. 18. Retrieved relative difference of total column carbon monoxide amount utilizing processing with an artificial 0.1% negative bias introduced in the surface pressure measurements, and with the SZA-induced bias removed from the final data (colour online)

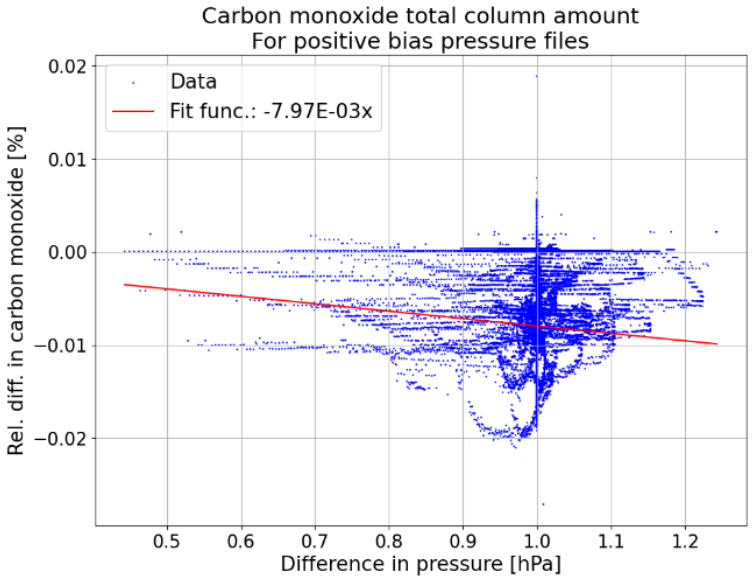

Fig. 19. Retrieved relative difference of total column carbon monoxide amount utilizing processing with an artificial 0.1% positive bias introduced in the surface pressure measurements, and with the SZA-induced bias removed from the final data (colour online)

4.4. Water vapor retrieval results

A similar trend to the other GHGs is to be observed with water vapor total column amount – its retrieval depends inversely on the surface pressure measurements, lower surface pressure inputs leading to higher retrieved values. This is highlighted in the offset-processed cases, where a ± 1 hPa offset leads to a $\mp 0.040\%$ difference in the final retrieved quantities.

Considering eq. (6), this leads to a scaling factor:

$$S = \frac{\mu_{RD}}{\Delta p} = \frac{0.040\%}{hPa} \tag{23}$$

These findings are in accordance with the results from the bias-processed files. These correlate well with the offset-processed results, highlighting, utilizing eq. (5), a linear fit function with the following formula:

$$RD = -3.98 \cdot 10^{-2} \cdot \Delta p \ [\%] \tag{24}$$

Worth noting is the fact that intraday variability for water vapor is significantly higher than for other GHGs, so the spread of the points of the graph is more visible. However, Figs. 21, 22, 23 and 24 indicate a good stability in the retrieval algorithm, as the 1:1 line and the linear fit are almost perfectly overlapping.

The very similar linear fitting parameters are also to be noted, but these do not necessarily contain inherently useful information. This is because the fitting of modified values

(represented by y) is done to the originally retrieved values (represented by x), thus being different (and unquantifiable so) for each different set of surface pressure measurements used to process the data.

Further study is required for a proper characterization of the relationship between the fitting parameters from the offset-processed cases and those in Figs. 21, 22, 23 and 24.

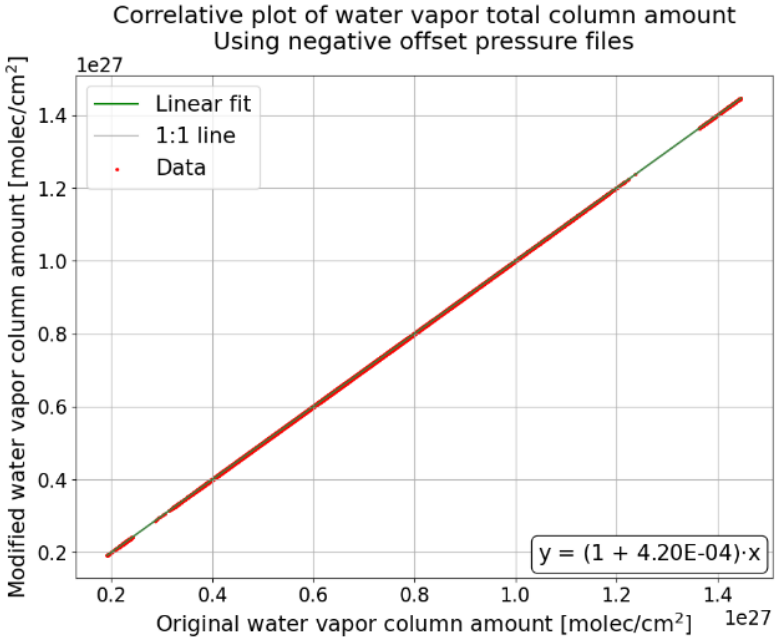

Fig. 20. Correlative plot of total column water vapor amount utilizing processing with an artificial 1 hPa negative offset introduced in the surface pressure measurements, compared to the originally retrieved quantities (colour online)

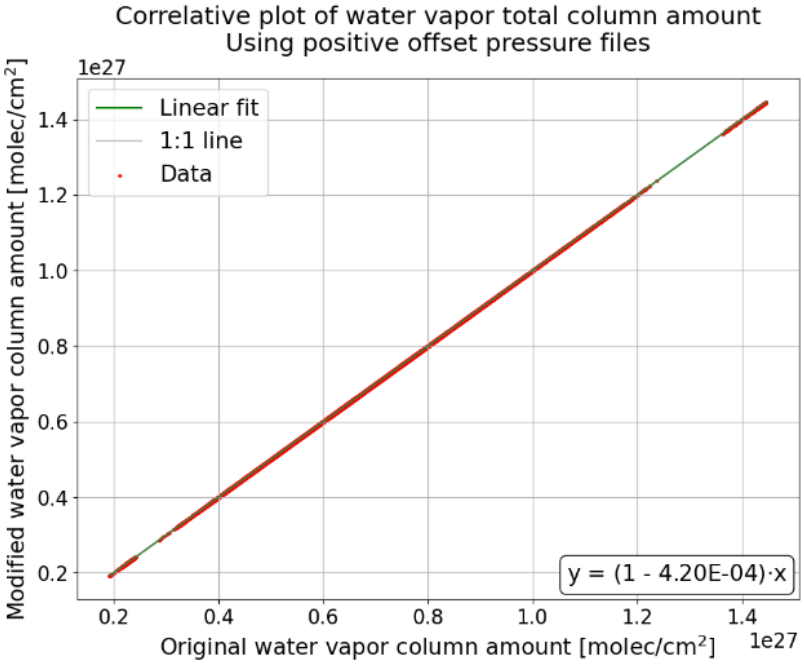

Fig. 21. Correlative plot of total column water vapor amount utilizing processing with an artificial 1 hPa positive offset introduced in the surface pressure measurements, compared to the originally retrieved quantities (colour online)

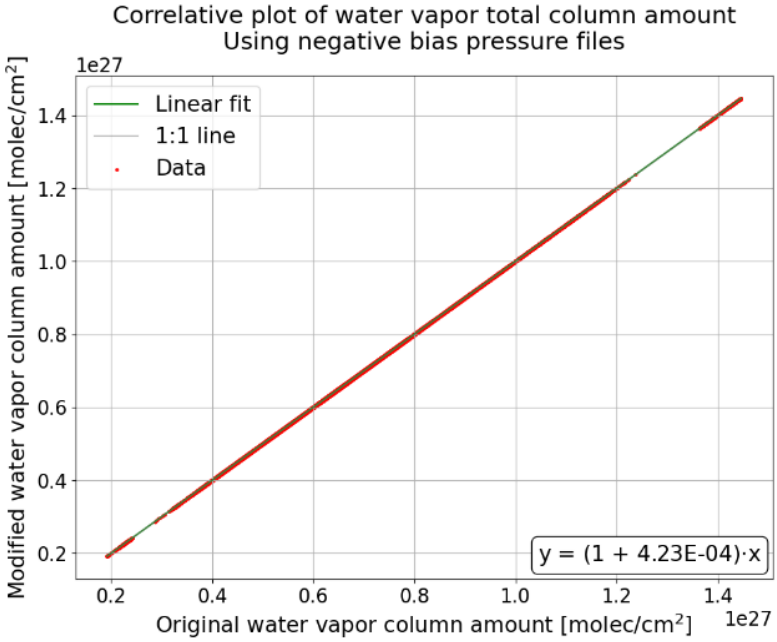

Fig. 22. Correlative plot of total column water vapor amount utilizing processing with an artificial 0.1% negative bias introduced in the surface pressure measurements, compared to the originally retrieved quantities (colour online)

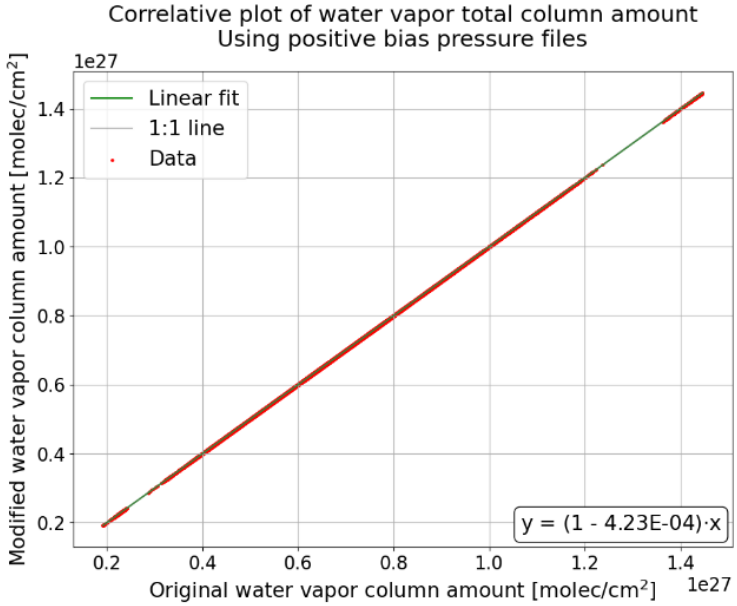

Fig. 23. Correlative plot of total column water vapor amount utilizing processing with an artificial 0.1% positive bias introduced in the surface pressure measurements, compared to the originally retrieved quantities (colour online)

When analyzing the symmetry and linearity of the H_2O retrieval for a $\pm$50 hPa offset, mean relative differences of +2.059% (for a -50 hPa offset) and -1.927% (for a +50 hPa offset), respectively.

By utilizing eq. (6), two scaling factors, one for each case, are obtained:

$$S_{positive-offset} = \frac{-1.927\%}{50} \approx -0.039 \left[\frac{\%}{hPa}\right] \quad (25)$$

$$S_{negative-offset} = \frac{2.059\%}{-50} = -0.041 \left[\frac{\%}{hPa}\right] \quad (26)$$

A slight asymmetry between the two scaling factors is to be observed, which signifies a slight deviation from the linear dependency we observed in the $\pm$1 hPa offset-processed retrievals. This can be attributed to the higher variability of water vapor compared to the other GHGs, or particular sensitivities in the spectral ranges used for the retrieval of H_2O, but requires a more in-depth study to draw concrete conclusions. However, a mean scaling factor is still offered by eq. (10):

$$S_{big-offset} = \frac{-0.039 - 0.041}{2} = -0.040 \left[\frac{\%}{hPa}\right] \quad (27)$$

Which is very similar to the one presented in eq. (22), indicating that the variations from the linear dependency are not very high.

Additionally, the study of random bias-processed files highlights a mean standard deviation of $7.82 \cdot 10^{22}$ molec/cm^2 and a mean value of $6.92 \cdot 10^{26}$ molec/cm^2. The results of the processing can be seen in Fig. 24.

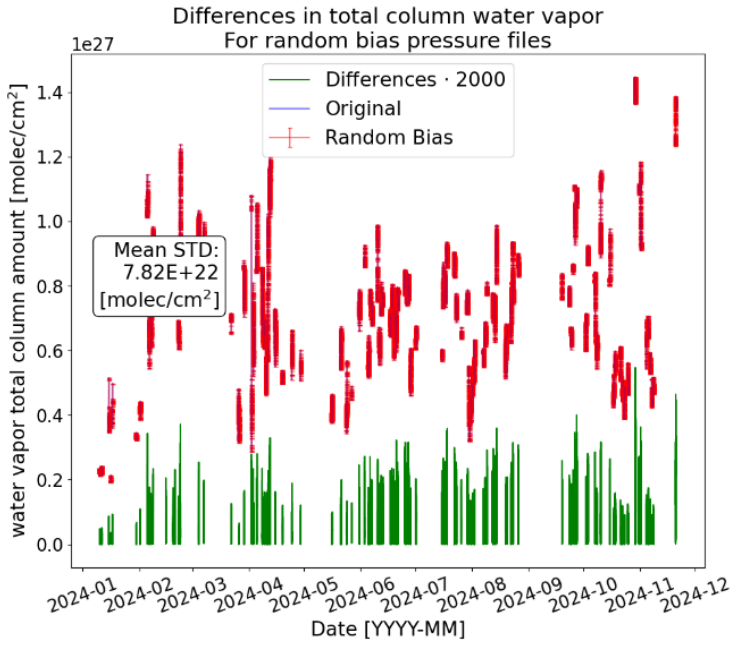

Fig. 24. Retrieved relative difference of total water vapor amount utilizing processing with an artificial 0.05% random bias introduced in the surface pressure measurements (colour online)

The value of the mean standard deviation can be utilized alongside eq. (7) to obtain a value for the relative standard deviation:

$$\sigma_{RD} = \frac{\sigma_X}{\mu_X} \approx 1.13 \cdot 10^{-2} \ [\%] \quad (28)$$

Also included are results for the $\pm 0.1\%$ bias-processed files with the solar zenith angle dependency removed, present in Figs. 25 and 26.

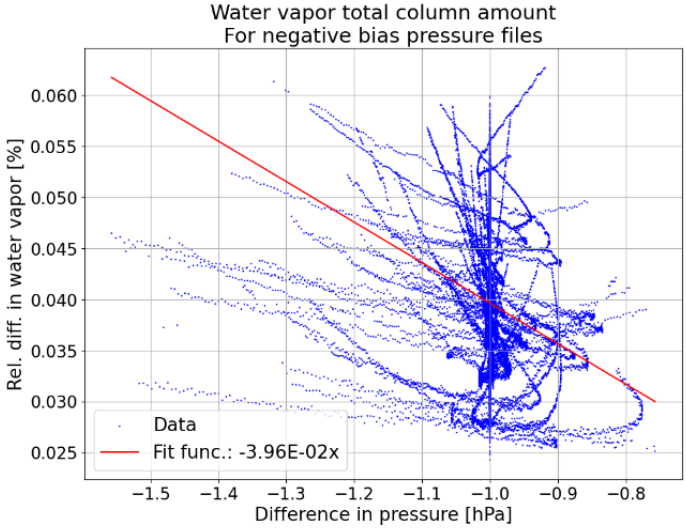

Fig. 25. Retrieved relative difference of total column water vapor amount utilizing processing with an artificial 0.1% negative bias introduced in the surface pressure measurements, and with the SZA-induced bias removed from the final data (colour online)

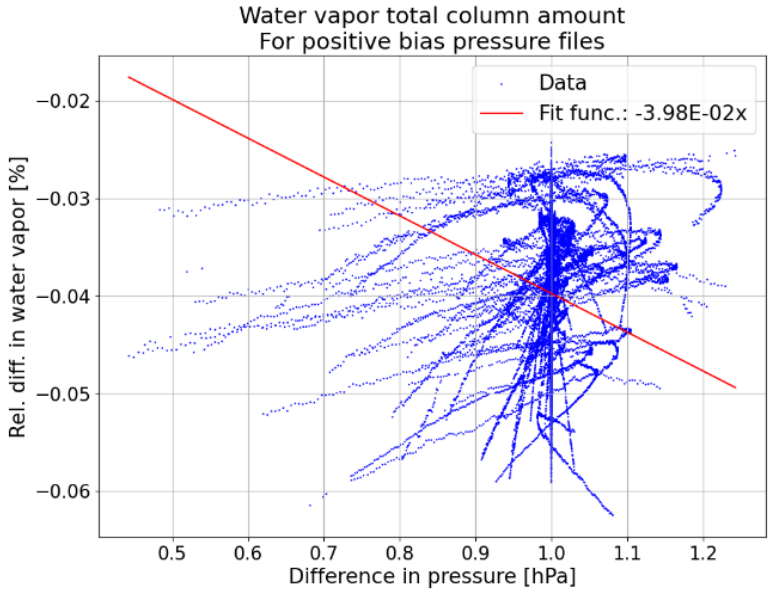

Fig. 26. Retrieved relative difference of total column water vapor amount utilizing processing with an artificial 0.1% positive bias introduced in the surface pressure measurements, and with the SZA-induced bias removed from the final data (colour online)

These show a good correlation with the results present in the unmodified bias-processed files, and have very similar fit parameters as those present in eq. (24), suggesting the variation induced by the difference in surface pressure is significant even without the effect of solar zenith angle.

5. Conclusions

For all the studied greenhouse gases, there is a clear inverse dependency in the assumed surface pressure values and the retrieved quantities.

Furthermore, for a ± 1 hPa variation interval of pressure, the dependency also features a linear behaviour for all GHGs. This appears to be extendable to a ± 50 hPa interval for CO, CO_2 and CH_4 retrievals, as the scaling factors determined for each are stable with a higher offset in pressure. Water vapor, however, presents a more powerful asymmetry between the negative and positive offset cases, so more study is required to ensure the linear approximation is still valid for this higher interval of variation.

Using the linear dependence of the retrieved quantity of GHGs to the surface pressure measurements, and taking into account the COCCON recommended necessary precision for pressure measurements (± 0.2 hPa [15]), an assessment of the uncertainties arising from the uncertainty in pressure are presented below:

Table 1. Table with results from the sensitivity study on pressure

GHG	σ_{1hPa} [%]	$\sigma_{0.2hPa}$ [%]	σ_{SoA} [%]	σ_{Rel} [%]
CO_2	0.018	0.003	0.24	1.25
CH_4	0.014	0.003	0.18	1.67
CO	0.008	0.002	-	-
H_2O	0.040	0.008	-	-

where σ_{1hPa} is the uncertainty when a variation of ± 1 hPa is considered in the surface pressure measurements, $\sigma_{0.2hPa}$ is the uncertainty for a ± 0.2 hPa variations (as per the network standards), σ_{SoA} is the state of the art estimated uncertainty for the instrument's precision and σ_{Rel} is the relative proportion of uncertainty coming from the associated surface pressure measurements' uncertainties. This was calculated with the formula:

$$\sigma_{Rel} = \frac{\sigma_{0.2hPa}}{\sigma_{SoA}} \cdot 100\ [\%] \tag{29}$$

Considering, in practice, a surface pressure sensor with a worse precision (assumed to be ± 1 hPa), an estimation for the uncertainty of the instrument then becomes:

$$\sigma_{Inst} = \sigma_{SoA} - \sigma_{0.2hPa} + \sigma_{1hPa} \tag{30}$$

Applying the same reasoning as in eq. (29), we obtain new estimates for the relative uncertainty provided by an uncertainty in the surface pressure measurements for each GHG:

$$\sigma_{Rel_{CO_2}} = \frac{\sigma_{1hPa_{CO_2}}}{\sigma_{Inst_{CO_2}}} \approx 9.23\ [\%] \quad (31)$$

$$\sigma_{Rel_{CH_4}} = \frac{\sigma_{1hPa_{CH_4}}}{\sigma_{Inst_{CH2}}} \approx 7.33\ [\%] \quad (32)$$

Furthermore, considering the statistical nature of the processing chain, for the random-bias processing cases of each GHG, the expected relative standard deviation can be approximated as:

$$\sigma_{RD_{theoretical}} = |S|\sqrt{Var(p)} \quad (33)$$

where $|S|$ is the scaling factor derived from each offset-processed rerun, and $Var(p)$ is the variance of the associated pressure variable, derived using the formula for the variance of a uniformly distributed variable:

$$Var(p) = \frac{(H-L)^2}{12} \approx 0.083\ [hPa] \quad (34)$$

where H is the pressure upper bound (+0.5hPa) and L is the pressure lower bound (-0.5hPa).

Therefore, for each GHG, we can compute a theoretical value of the expected mean relative standard deviation. If the theoretical value is similar to the experimentally obtained one, we can ensure that the hypothesis of a linear dependency is valid. The results are shown below, in Table 2.

Table 2. Table with results from the statistical analysis of the bias-processed cases

GHG	$\sigma_{RD_{experimenta}}$ [%]	$\sigma_{RD_{theoretical}}$ [%]	$\lvert\sigma_{RD_{difference}}\rvert$ [%]
CO_2	$4.91 \cdot 10^{-3}$	$5.20 \cdot 10^{-3}$	$0.29 \cdot 10^{-3}$
CH_4	$3.81 \cdot 10^{-3}$	$4.04 \cdot 10^{-3}$	$0.23 \cdot 10^{-3}$
CO	$2.34 \cdot 10^{-3}$	$2.31 \cdot 10^{-3}$	$0.03 \cdot 10^{-3}$
H_2O	$1.13 \cdot 10^{-2}$	$1.15 \cdot 10^{-2}$	$0.02 \cdot 10^{-2}$

The absolute differences of the experimental and theoretical mean relative standard deviation values are small, indicating that the dependency is indeed linear, at least for the ± 0.5 hPa interval, in which the random-bias processed case study was done. Therefore, alongside all of the other evidence presented in this paper, a proposal of a post-processing surface pressure uncertainty correction function is made, for each GHG, expressed in molec/cm^2:

$$X_{CO_2} = (1 + 1.75 \cdot 10^{-4} \cdot \Delta p) \cdot X_{0_{CO_2}} \quad (35)$$

$$X_{CH_4} = (1 + 1.37 \cdot 10^{-4} \cdot \Delta p) \cdot X_{0_{CH_4}} \quad (36)$$

$$X_{CO} = (1 + 7.94 \cdot 10^{-5} \cdot \Delta p) \cdot X_{0_{CO}} \quad (37)$$

$$X_{H_2O} = (1 + 3.98 \cdot 10^{-4} \cdot \Delta p) \cdot X_{0_{H_2O}} \quad (38)$$

Additionally, new values for the estimated uncertainty of the final retrieved quantities are proposed, taking into account the associated uncertainty provided by the pressure sensor utilized for the gathering of surface pressure data. These are computed with the following formula:

$$\sigma_X = \sigma_{SoA} - \sigma_{0.2hPa} + \sigma_{n\ hPa} \quad (39)$$

where $\sigma_{n\ hPa}$ is the associated mean standard standard deviation coming from an uncertainty of n hPa in the assumed surface pressure measurements, taken as a uniform distribution (equivalent to random noise). These estimates, when expressed in percentages, then become:

$$\sigma_{CO_2} \approx n^2 \cdot 6.24 \cdot 10^{-4} + 0.24 \quad (40)$$

$$\sigma_{CH_4} \approx n^2 \cdot 4.85 \cdot 10^{-4} + 0.18 \quad (41)$$

Compared to other state of the art results for the total uncertainty attributed to the associated pressure uncertainty in the CO_2 retrieval, the results found in this paper are in line with estimates found in [24]. This takes into account the additional errors found in XCO_2 (mixing ratio) retrievals, compared to CO_2 (total column) retrievals, as implied by eq. (2). However, [11] finds a different result, with a stated 0.19% bias for $\pm$3mbar, equating to approximately $\frac{0.063\%}{hPa}$ difference for total column measurements. This difference could be attributed to differences in software version or statistical analysis methods utilized, but requires further study for a proper conclusion to be drawn. Moreover, other factors that have not been accounted in this study contribute to additional uncertainties in the final results. These factors include the seasonal component present in GHG column amounts which cannot be statistically be removed due to lack of multiple years of data (only a time-span of 1 year, consisting of 107 days of measurements, was studied) and the presumption of how failure modes/characteristics of pressure sensors affect the retrieved surface pressure values, which may be different than real-life behavior of such poor-performing equipment.

Acknowledgements

This work was carried out through the Core Program within the National Research Development and Innovation Plan 2022-2027, carried out with the support of MCID, project no. PN 23 05 and by the IM4CA (www.im4ca.eu) project supported by the European Commission under the Horizon Europe (HORIZON), Grant Agreement: 101183460.

Further support was provided by the European Regional Development Fund through the Competitiveness Operational Programme 2014–2020, Action 1.1.3 Creating synergies with H2020 Programme, project H2020 Support Centre for European project management and European promotion, MYSMIS code 107874 (ctr. no. 253/2.06.2020) and by the project Strengthen the participation of the ACTRIS-RO consortium in the pan-European research

infrastructure ACTRIS, ACTRIS-ROC, MYSMIS code 107596 (ctr. no.337/2021).

References

[1] V. Nicolae, L. Belegante, J. Vasilescu, A. Nemuc, F. Toanca, O. G. Tudose, C. Radu, D. Nicolae, J. Optoelectron. Adv. M. **25**(3-4), 176 (2023).
[2] E. Carstea, K. Fragkos, Optoelectron. Adv. Mat. **18**(11-12), 562 (2024).
[3] M. Zoran, D. Savastru, S. Miclos, M. N. Tautan, L. Baschir, J. Optoelectron. Adv. M. **13**(9-10), 1159 (2011).
[4] K. Calvin, D. Dasgupta, G. Krinner, A. Mukherji, P. W. Thorne, C. Trisos, J. Romero, P. Aldunce, K. Barrett, G. Blanco, W. W. L. Cheung, S. Connors, F. Denton, A. Diongue-Niang, D. Dodman, M. Garschagen, O. Geden, B. Hayward, C. Jones, F. Jotzo, T. Krug, R. Lasco, Y.-Y. Lee, V. Masson-Delmotte, M. Meinshausen, K. Mintenbeck, A. Mokssit, F. E. L. Otto, M. Pathak, A. Pirani, E. Poloczanska, H.-O. Pörtner, A. Revi, D. C. Roberts, J. Roy, A. C. Ruane, J. Skea, P. R. Shukla, R. Slade, A. Slangen, Y. Sokona, A. A. Sörensson, M. Tignor, D. Van Vuuren, Y.-M. Wei, H. Winkler, P. Zhai, Z. Zommers, J.-C. Hourcade, F. X. Johnson, S. Pachauri, N. P. Simpson, C. Singh, A. Jhomas, E. Totin, P. Arias, M. Bustamante, I. Elgizouli, G. Flato, M. Howden, C. Méndez-Vallejo, J. J. Pereira, R. Pichs-Madruga, S. K. Rose, Y. Saheb, R. Sánchez Rodríguez, D. Ürge-Vorsatz, C. Xiao, N. Yassaa, A. Alegría, K. Armour, B. Bednar-Friedl, K. Blok, G. Cissé, F. Dentener, S. Eriksen, E. Fischer, G. Garner, C. Guivarch, M. Haasnoot, G. Hansen, M. Hauser, E. Hawkins, T. Hermans, R. Kopp, N. Leprince-Ringuet, J. Lewis, D. Ley, C. Ludden, L. Niamir, Z. Nicholls, S. Some, S. Szopa, B. Trewin, K.-I. Van Der Wijst, G. Winter, M. Witting, A. Birt, M. Ha, J. Romero, J. Kim, E. F. Haites, Y. Jung, R. Stavins, A. Birt, M. Ha, D. J. A. Orendain, L. Ignon, S. Park, Y. Park, A. Reisinger, D. Cammaramo, A. Fischlin, J. S. Fuglestvedt, G. Hansen, C. Ludden, V. Masson-Delmotte, J. B. R. Matthews, K. Mintenbeck, A. Pirani, E. Poloczanska, N. Leprince-Ringuet, and C. Péan, "IPCC, 2023: Climate Change 2023: Synthesis Report. Contribution of Working Groups I, II and III to the Sixth Assessment Report of the Intergovernmental Panel on Climate Change [Core Writing Team, H. Lee, J. Romero (eds.)]. IPCC, Geneva, Switzerland., Intergovernmental Panel on Climate Change (IPCC), 2023.
[5] UNFCCC, The Paris Agreement, presented at the Paris Climate Change Conference - November 2015, Paris: UNFCCC, Nov. 2018.
[6] UNFCCC, The Global Methane Pledge, presented at the The UN Climate Change Conference in Glasgow, Glasgow: UNFCCC, Nov. 2021. Accessed: Feb. 17, 2025.
[7] V. V. Rozanov, A. V. Rozanov, Atmos. Meas. Tech. 3(3), 751 (2010).
[8] Differential Absorption Lidar - an overview | ScienceDirect Topics.
[9] D. Nicolae, C. P. Cristescu, J. Optoelectron. Adv. M. **8**(5), 1781 (2006).
[10] R. E. Mamouri, A. Papayannis, G. Tsaknakis, V. Amiridis, J. Optoelectron. Adv. M. **9**(11), 3546 (2007).
[11] Matthias Max Frey, Nature Science Doctorate, Faculty of Physics from Karlsruhe Institute for Technology (KIT), 2018.
[12] A. Dandocsi, L. Marmureanu, C. Marin, N. Puscas, University Politehnica of Bucharest Scientific Bulletin-Series A-Applied Mathematics And Physics **81**(2), 201 (2019).
[13] C. Alberti, F. Hase, D. Dubravica, A. Dehn, P. Castracane, The COllaborative Carbon Column Observing Network (COCCON) quality management.
[14] M. K. Sha, Saswati Das, Matthias M. Frey, Darko Dubravica, Carlos Alberti, Bianca C. Baier, Dimitrios Balis, Alejandro Bezanilla, Thomas Blumenstock, Hartmut Boesch, Zhaonan Cai, Jia Chen, Alexandru Dandocsi, Martine De Mazière, Stefani Foka, Omaira García, Lawson David Gillespie, Konstantin Gribanov, Jochen Gross, Michel Grutter, Philip Handley, Frank Hase, Pauli Heikkinen, Neil Humpage, Nicole Jacobs, Sujong Jeong, Tomi Karppinen, Matthäus Kiel, Rigel Kivi, Bavo Langerock, Joshua Laughner, Morgan Lopez, Maria Makarova, Marios Mermigkas, Isamu Morino, Nasrin Mostafavipak, Anca Nemuc, Timothy Newberger, Hirofumi Ohyama, William Okello, Gregory Osterman, Hayoung Park, Razvan Pirloaga, David F. Pollard, Uwe Raffalski, Michel Ramonet, Eliezer Sepúlveda, William R. Simpson, Wolfgang Stremme, Colm Sweeney, Noemie Taquet, Chrysanthi Topaloglou, Qiansi Tu, Thorsten Warneke, Debra Wunch, Vyacheslav Zakharov, Minqiang Zhou, Remote Sensing **17**(5), 734 (2025).
[15] PROFFAST User Manual, Karlsruhe Institute for Technology, Dec. 2023.
[16] Lena Feld Benedikt Herkommer, PROFFASTpylot v1.3 documentation, Karlsruhe Institute for Technology, Dec. 2023.
[17] T. E. L. Smith, M. J. Wooster, M. Tattaris, D. W. T. Griffith, Atmos. Meas. Tech. **4**(1), 97 (2011).
[18] E. Guillaume, L. Saragoza, K. Wakatsuki, P. Blomqvist, Fire and Materials **39**(7), 675 (2015).
[19] EM27/SUN Solar Absorption Spectrometer.
[20] Qiansi Tu, Darko Dubravica, Benedikt Herkommer, Lena Feld, Frank Hase, PROFFASTpylot. (Apr. 22, 2024), Python. Karlsruhe Institute for Technology.
[22] I. (STS) Oberdorf, KIT.
[23] M. Gisi, F. Hase, S. Dohe, T. Blumenstock, A. Simon, A. Keens, Atmos. Meas. Tech. **5**(11), 2969 (2012).

[24] J. K. Hedelius, Camille Viatte, Debra Wunch, Coleen M. Roehl, Geoffrey C. Toon, Jia Chen, Taylor Jones, Steven C. Wofsy, Jonathan E. Franklin, Harrison Parker, Manvendra K. Dubey, Paul O. Wennberg, Atmos. Meas. Tech. **9**(8), 3527 (2016).
[25] D. Wunch, Geoffrey C. Toon, Jean-François L. Blavier, Rebecca A. Washenfelder, Justus Notholt, Brian J. Connor, David W. T. Griffith, Vanessa Sherlock, Paul O. Wennberg, Phil. Trans. R. Soc. A **369**(1943), 2087 (2011).
[26] Magurele center for Atmosphere and Radiation Studies (MARS) - environment.inoe.ro.
[27] L. Belegante, C. Talianu, A. Nemuc, V. Nicolae, G. Ciocan, F. Toanca, O. G. Tudose, C. Radu, D. Nicolae, J. Optoelectron. Adv. M. **26**(9-10), 422 (2024).
[28] R. Pîrloagă, M. Adam, B. Antonescu, S. Andrei, S. Ştefan, Remote Sensing **15**(6), 1514 (2023).
[29] B. Herkommer, KIT-IMKASF - About IMKASF - Research Groups - Ground-Based Remote Sensing - COCCON - Data Processing.
[30] M. K. Sha, Martine De Mazière, Justus Notholt, Thomas Blumenstock, Huilin Chen, Angelika Dehn, David W. T. Griffith, Frank Hase, Pauli Heikkinen, Christian Hermans, Alex Hoffmann, Marko Huebner, Nicholas Jones, Rigel Kivi, Bavo Langerock, Christof Petri, Francis Scolas, Qiansi Tu, Damien Weidmann, Atmos. Meas. Tech. **13**(9), 4791 (2020).
[31] P. C. Logofatu, D. Apostol, J. Optoelectron. Adv. M. **9**(9), 2838 (2007).
[32] V. Nascov, P. C. Logofatu, D. Apostol, J. Optoelectron. Adv. M. **12**(6), 1311 (2010).
[33] Base Package, https://www.bruker.com/en/products-and-solutions/infrared-and-raman/opus-spectroscopy-software/base-package.html
[34] GMAO - Global Modeling and Assimilation Office Research Site, https://gmao.gsfc.nasa.gov/GMAO_products/NRT_products.php
[35] RunningGGG2020 < Main < TCCON Wiki, https://tccon-wiki.caltech.edu/Main/RunningGGG2020
[36] HOBO S-BPB-CM50 Barometric Pressure Smart Sensor, https://www.weathershop.co.uk/s-bpb-cm50-barometric-pressure-smart-sensor-1
[37] PE-8000, Paragon Controls. https://paragoncontrols.com/products/pe-8000-outside-pressure-outdoor-pressure-sensor/
[38] Barometric Pressure Sensors | Barometers for Sale | Scientific Sales | Young 61402L | Young Barometric Pressure Sensor, Scientific Sales, Inc. Available: https://www.scientificsales.com/product-p/61402l.htm
[39] Pressure Broadening - an overview | ScienceDirect Topics, https://www.sciencedirect.com/topics/earth-and-planetary-sciences/pressure-broadening
[40] D. Dubravica, KIT-IMKASF - About IMKASF - Research Groups - Ground-Based Remote Sensing - COCCON - Instrument, https://www.imk-asf.kit.edu/english/3233.php
[41] Welcome to Python.org, Python.org., https://www.python.org/
[42] J. T. VanderPlas, ApJS 236(1), 16 (2018).
[43] K. Thoning, E. Dlugokencky, X. Lan, NOAA Global Monitoring Laboratory, NOAA GML, 2022.
[44] C. Sweeney, Anna Karion, Sonja Wolter, Timothy Newberger, Doug Guenther, Jack A. Higgs, Arlyn Elyzabeth Andrews, Patricia M. Lang, Don Neff, Edward Dlugokencky, John B. Miller, Stephen A. Montzka, Ben R. Miller, Ken Alan Masarie, Sebastien Christophe Biraud, Paul C. Novelli, Molly Crotwell, Andrew M. Crotwell, Kirk Thoning, Pieter P. Tans, JGR Atmospheres **120**(10), 5155 (2015).
[45] Air Mass Formula, https://www.ftexploring.com/solar-energy/air-mass-and-insolation2.htm
[46] Carbon Monoxide - an overview | ScienceDirect Topics, https://www.sciencedirect.com/topics/earth-and-planetary-sciences/carbon-monoxide

*Corresponding author: alexandru.dandocsi@inoe.ro